J Membrane Biol (2007) 216:83–92
DOI 10.1007/s00232-007-9037-9

Imaging and Force Spectroscopy on Desmoglein 1 Using Atomic Force Microscopy Reveal Multivalent Ca^{2+}-Dependent, Low-Affinity *Trans*-Interaction

Jens Waschke · Carlos Menendez-Castro · Paola Bruggeman · Rainer Koob · Masayuki Amagai · Hermann J. Gruber · Detlev Drenckhahn · Werner Baumgartner

Received: 24 January 2007 / Accepted: 14 May 2007 / Published online: 27 July 2007

Abstract Desmoglein 1 is a desmosomal member of the cadherin family expressed in stratified epithelia. Desmoglein 1 is the target adhesion molecule of severe blistering skin diseases such as pemphigus or bullous impetigo. However, despite this enormous pathological relevance, the molecular binding properties of desmoglein 1 are largely unknown. Using atomic force microscopic imaging, we found that desmoglein 1 molecules displayed Ca^{2+}-dependent conformational changes of the extracellular domains. By single-molecule force-distance cycles, we provide evidence that desmoglein 1 undergoes Ca^{2+}-dependent (K_d = 0.8 mM Ca^{2+}) homophilic *trans*-interaction, which is highly relevant for the contribution of desmoglein 1 homophilic binding to keratinocyte cohesion in distinct epidermal layers. Moreover, while the single-unit unbinding force is comparable to other cadherins (~40 pN at retrace velocity of 300 nm/s), apparent differences with respect to multivalency of interaction and lifetime of single bonds (0.17 s) were observed. Thus, besides the biophysical characterization of desmoglein 1, a main outcome of the study is that desmoglein 1 differs from other members of the cadherin family in terms of some molecular binding properties.

Keywords Desmosome · Atomic force microscopy · Pemphigus · Cadherin · Cell adhesion

Introduction

Desmosomes are specialized adhesive intercellular junctions mainly confined to epithelial cells of simple and multilayered epithelia, where they serve to stabilize the epithelial barrier and protect it against mechanical shear forces (Garrod, Merritt & Nie, 2002; Kottke, Delva & Kowalczyk, 2006). The most obvious pathological consequence of impaired desmosomal function is known as pemphigus disease, a life-threatening blistering of the epidermis and in certain cases of the upper alimentary system (mouth, esophagus) (Amagai, 2003; Bystryn & Rudolph, 2005; Payne et al., 2004; Stanley & Amagai, 2006). Pemphigus is caused by autoantibodies against desmoglein-type desmosomal adhesion molecules, which belong to the cadherin superfamily (Sitaru & Zillikens, 2005). In contrast to other classical cadherins, in epithelial cells the cytodomains of desmogleins are anchored to intermediate filaments of the cytokeratin family via adaptor proteins such as plakoglobin and desmoplakin (Garrod et al., 2002; Kottke et al., 2006). In humans, the desmoglein family consists of four related members, i.e., desmogleins 1, 2, 3 and 4 (Dsg1, -2, -3, -4) (Kottke et al., 2006).

Jens Waschke, Carlos Menendez-Castro, and Paola Bruggeman contributed equally to this study.

J. Waschke · C. Menendez-Castro · P. Bruggeman · R. Koob · D. Drenckhahn (✉) · W. Baumgartner
Institute of Anatomy and Cell Biology, University of Würzburg, Koellikerstrasse 6, Würzburg D-97070, Germany
e-mail: anat015@mail.uni-wuerzburg.de

M. Amagai
Department of Dermatology, Keio University School of Medicine, 35 Shinanomachi Shinjuku-ku, Tokyo 160-8582, Japan

H. J. Gruber
Institute of Biophysics, University of Linz, Altenbergerstrasse 69, Linz 4040 , Austria

W. Baumgartner
Department of Cellular Neurobionics, Institute of Biology 2, Rheinisch-Westfälische Technische Hochschule Aachen, Kopernikusstrasse 6, Aachen D-52056, Germany

Autoantibodies directed to the ectodomain of Dsg1 are the main cause of pemphigus foliaceus, and a combination of autoantibodies to Dsg1 and Dsg3 causes the even more severe pemphigus vulgaris (Bystryn & Rudolph, 2005; Mahoney et al., 1999; Miyagawa et al., 1999). In bullous impetigo, Dsg1 is selectively cleaved by bacterial proteases (Amagai et al., 2000; Payne et al., 2004; Stanley & Amagai, 2006). This defines Dsg1 as a clinically highly important member of desmosomal cadherins. Recently, we have shown by single-molecule atomic force microscopy (AFM) that Dsg1-specifc autoantibodies in pemphigus foliaceus do not directly interfere with Dsg1 *trans*-interaction but rather induce cellular mechanisms (Waschke et al., 2005) and identified that Rho guanosine triphosphatases (GTPases) are involved in the signaling events leading to keratinocyte dissociation and epidermal splitting (Waschke et al., 2006).

Despite the biological and clinical importance of Dsg1, its binding properties have not been elucidated so far. Like in all other conventional cadherins, the adhesive ectodomain of desmogleins consists of five homologous subdomains, EC 1-5, that require Ca^{2+} for structural stability and adhesive activity (Garrod et al., 2002; Kottke et al., 2006). Three-dimensional reconstruction based on electron micrographs of the intercellular cleft of desmosomes indicated assembly of the ectodomains in which the outermost EC 1 subdomains of neighboring desmosomal cadherins associate laterally by *cis*-interaction and additionally bind to opposing molecules by *trans*-interaction (He, Cowin & Stokes, 2003).

In the present study, we characterized molecular binding properties of Dsg1 by AFM using dimers of entire extracellular domains of human Dsg1 fused to the Fc portion of human immunoglobulin G (Dsg1-Fc). We show by AFM imaging that the ectodomain of Dsg1 requires almost millimolar concentrations of Ca^{2+} to form straight rod-shaped *cis* dimers, which, in the absence of Ca^{2+}, separate into diverging single stands. Force spectroscopy of *trans*-interacting Dsg1 molecules showed single-unit unbinding events, comparable in strength to other cadherin-type molecules. In addition, higher-order unbinding events were recorded, suggesting changing degrees of overlap between *trans*-interacting external domains with cumulative binding strength.

Materials and Methods

Recombinant Dsg1-Fc

Dsg1-Fc was expressed by stably transfected Chinese hamster ovary (CHO) cells and purified from culture supernatants by affinity chromatography exactly as described previously (Waschke et al., 2005).

AFM

For imaging of hydrated Dsg1-Fc, the chimeric proteins were covalently coupled to a gold-linked self-assembled monolayer (SAM) in the presence or absence of Ca^{2+}. For this purpose, freshly cleaved mica sheets were sputter-coated, yielding a gold layer of approximately 150 nm thickness. In order to obtain ultraflat gold surfaces, flame annealing was performed. The surface was checked by AFM imaging, and if the desired flatness of the gold surface was not reached, flame annealing was repeated. For formation of a SAM, the gold-coated mica sheets were incubated with a 1 mM solution of a 1:500 mixture of liponic acid and liponic acid amide in ethanol for 2 h. After rinsing twice for 5 min with ethanol and twice with dimethyl formamide (DMF), the carboxyl groups of the liponic acid were activated by incubation with 1 mM*N*-hydroxy-succimide (NHS), 1 mM diisopropylcarbodiimide, 1 mM *N*,*N*-Diisoporpylethylamine (DIPEA) and 0.2 mM Dimethylaminopyridin (DMAP) in DMF for 3 h at room temperature. Afterward, the mica sheets were washed twice for 5 min with DMF, followed by MeOH and then H_2O. Then, the sheets were incubated with the Dsg1-Fc chimeric protein at a concentration of approximately 0.03 ng/l in 4-(2-hydroxyethyl)-1-piperazineethanesulfonic acid (HEPES) buffer (10 mM HEPES, 150 mM NaCl, pH 7.4) containing 2 mM of either $CaCl_2$ or ethyleneglycoltetraacetic acid (EGTA) for 15 min at room temperature. Then, the sheets were washed three times in a tris(hydroxymethyl)aminomethane (TRIS) buffer containing 10 mM TRIS, 150 mM NaCl and 2 mM of either $CaCl_2$ or EGTA. Imaging was performed in the TRIS buffer (with or without Ca^{2+}) using a Bioscope AFM driven by a Nanoscope III controller (Digital Instruments, Santa Barbara, CA) equipped with standard high reflective cantilevers (Park Scientific, Sunnyvale, CA). The nominal spring constant chosen was 10 pN/nm, and scanning force was adjusted to approximately 150 pN. Images were obtained in the contact mode. In order to avoid tip artefacts like double-tip effects, we typically prepared five SAMs for one experiment, one of which was not further treated, two of which were incubated with Dsg1 in Ca^{2+}-free buffer and two of which were incubated in Ca^{2+}-containing buffer. The typical sequence of one experiment was as follows. First, the tip was used for imaging a gold-grain standard (Park Scientific). If the tip was found appropriate, it was used for imaging of the SAM without protein. Afterwards, again using the same tip, imaging of the first Ca^{2+}-free sample was performed, followed by the

first Ca^{2+}-containing sample, the second Ca^{2+}-free sample and finally the second Ca^{2+}-containing sample. This procedure was repeated with another tip.

AFM Force Measurements

Dsg1-Dsg1 interactions were characterized by force-distance measurements of Dsg1 coupled via flexible linkers to the tip and substrate of the AFM. Dsg1 was linked covalently to the Si_3N_4 tip of the cantilever and freshly cleaved mica plates (Wacker, Burghausen, Germany) using polyethyleneglycol (PEG) spacers containing an amino-reactive crosslinker group (NHS ester) at one end and a thiol-reactive group (2-[pyridyldithio]propionate) at the other end, as described previously in detail (Hinterdorfer et al., 1996). The NHS group served to link PEG to free amino acid groups at both the Si_3N_4 tip and the SiOH plate introduced by treatment of the tip and plate with 2-aminoethanol HCl (Sigma, Taufkirchen, Germany). Binding events were measured in Hanks balanced salt solution (HBSS) by force-distance cycles at amplitudes of 300 nm and at frequencies ranging 0.5–10 Hz. Force-distance cycles were performed either at constant lateral positions or with lateral shifts of 1 nm/s. The spring constant of the cantilever in force measurements was 0.03 N/m. Force-distance cycles were analyzed as described previously in detail (Baumgartner & Drenckhahn, 2002; Baumgartner et al., 2003).

Synthesis of Lysine-*N*-Lipoic Acid-*N*-Aminohexylbenzophenone

In brief, all reaction steps were performed in a homemade glass column similar to the reaction vessel originally described by Merrifield (Merrifield, 1964; Wang & Merrifield, 1969). Standard procedures of solid-phase synthesis by the Fmoc strategy were used (Chan & White, 2003). Coupling reactions to form amide bonds were performed using HOBt/PyBOP activation of carboxylic acids.

N_α-Fmoc-N_ε-Mtt-lysine was coupled to Wang resin using the method of Sieber (Chan & White, 2003; Sieber, 1987). The Fmoc protecting group was removed by treatment with 20% piperidine in DMF, and *N*-Fmoc-aminocapronic acid was coupled to the α-amino group. After washing with dichloromethane (DCM) and removing the Fmoc group by piperidine as above, lipoic acid was coupled to the aminocapronic acid. The resin was washed with DCM and the Mtt group cleaved off with 1% trifluoroacetic acid (TFA)/1% Triisopropylsilane (TIS) in DCM. After several washes with DMF, *N*-Fmoc-aminocapronic acid was coupled. Deprotection with piperidine was followed by coupling of 4-benzoylbenzoic acid (B12407; Aldrich, Milwaukee, WI).

The compound was cleaved from the resin by 95% TFA in water, precipitated with ice-cold ether, and small amounts were purified on a semipreparative high-performance liquid chromatography Lichrosorb-C18 column using a 0.05% TFA/60% acetonitrile gradient.

Preparation of Lipoic Acid SAMs

Gold-sputtered mica sheets were washed several times with methanol and dried under a stream of nitrogen. The mica sheets were incubated with methanolic solutions containing 1 mM of lipoamide and 2 μM of lipoic acid or lysine-α -lipoic acid-ε-aminohexyl benzophenone for 2 h. After several rinses with dry DMF, activated NHS esters of lipoic acid residues were prepared by adding a DMF solution containing 1 mM NHS/1 mM *N*-ethyl-*N*'[3-(dimethylamino)propyl]carbodiimide hydrochloride (EDC)/0.1 mM DIPEA for 3 h.

To covalently attach proteins to the surface, DMF was washed away with HBSS and the protein solution immediately added to the mica sheets.

For the preparation of nitrilotriacetic acid (NTA) surfaces, the DMF was washed away with methanol and a 1 mM methanolic solution of *N,N*-bis-(carboxymethyl)-L-lysine (NTA-lysine) was added for 3 h. The mica sheets were rinsed several times with HBSS and stored in this buffer at 4°C. They were used within 1 week.

Mica sheets containing NTA-substituted lysine-α-lipoic acid-ε-aminohexyl benzophenone were used to covalently attach His-tagged proteins. Mica sheets were incubated with protein solutions, rinsed with HBSS and then irradiated with a 15-W ultraviolet (UV) lamp for 15 min from a distance of 5 cm.

Results

To investigate the molecular binding properties of Dsg1, we first characterized the Ca^{2+} dependence of homophilic Dsg1 binding.

Ca^{2+}-Dependent Conformational Changes of Dsg1

In a first step to characterize the Dsg1-Fc chimeric protein, we subjected the purified protein to AFM imaging. For this purpose, Dsg1-Fc was coupled covalently to an NHS-lipoic acid SAM as described above in the presence and absence of Ca^{2+}. The gold-supported SAM was found to be absolutely flat, resembling the topography of the underlying gold surface as evident in Figure 1A and B. Imaging of the hydrated but immobilized proteins in the absence of Ca^{2+} shows clearly visible structures on the SAM (Fig. 1C,D). At higher magnification, in the Ca^{2+}-free solution mostly

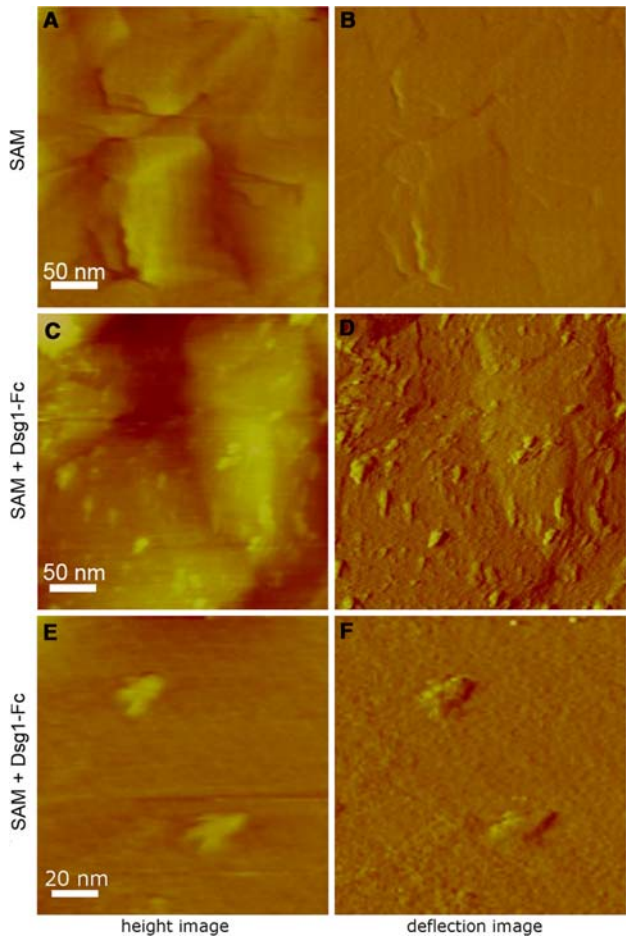

Fig. 1 Gold-supported SAM and attached Dsg1-Fc. AFM images of a gold-supported SAM in height mode (**A**), showing the actual topography in false colors, and in deflection mode (**B**). This is equivalent to a high pass filter or derivative of the height image and, therefore, presents small details with more contrast. These panels clearly show a very flat surface resembling the underlying gold topography. After incubation with Dsg1-Fc in the absence of Ca^{2+}, several small structures can be observed in height (**C**) and deflection (**D**) mode AFM. At higher magnification, Y-shaped proteins can be observed clearly (**E,F**). The apparent height of the individual proteins is about 3 nm when taking tip effects into account

Y-shaped structures were observed, which apparently reflected V-shaped spreading of the two extracellular domains of Dsg1 and the cross-linked Fc portions on the opposite end of the molecule (Fig. 1E,F). In the presence of Ca^{2+}, however, the structure of Dsg1-Fc molecules was rather different (Fig. 2), and exclusively rod-like structures could be observed, indicating *cis* dimer-like lateral association of the ectodomains.

Ca^{2+} Dependence of *Trans*-Interacting Dsg1

The Ca^{2+} dependence of binding of recombinant Dsg1-Fc was analyzed by AFM at various Ca^{2+} concentrations as described in detail previously for VE- and N-cadherin

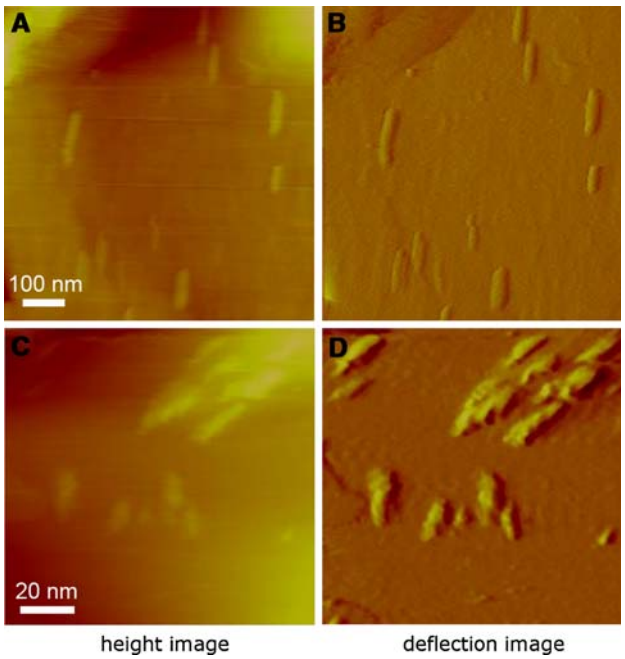

Fig. 2 Ca^{2+}-dependent conformational changes of Dsg1-Fc. AFM images of hydrated proteins bound to a gold-supported SAM in height mode (**A**, **C**) and in deflection mode (**B**, **D**). The proteins show a clear change from a Y shape (in the absence of Ca^{2+}, see Fig. 1) to a rod-like appearance, consistent with the hypothesis of Ca^{2+}-induced *cis*-dimerization. The apparent height of the individual proteins is about 3 nm

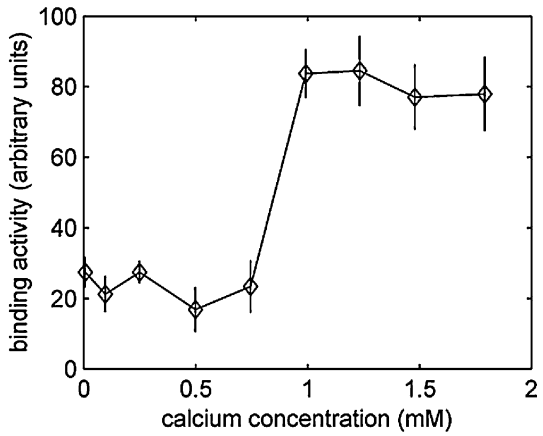

Fig. 3 Ca^{2+} dependence of Dsg1-Fc *trans*-interaction. Binding activity was determined using the AFM. Ca^{2+} dependence of binding activity (*trans*-interaction between tip- and substrate-bound Dsg1) showed half-maximal adhesion (apparent K_d) of 0.8 mM Ca^{2+} with a very high degree of cooperativity (Hill coefficient $n_h > 5$)

(Baumgartner et al., 2000, 2003). Approach-retrace cycles at $v_r = 800$ nm/s and 0.1 s encounter time were performed at different Ca^{2+} concentrations (0–10 mM). The total area between the force curve and the neutral line (position of undeflected cantilever) was taken as a measure of binding activity (Fig. 3). Each point of the

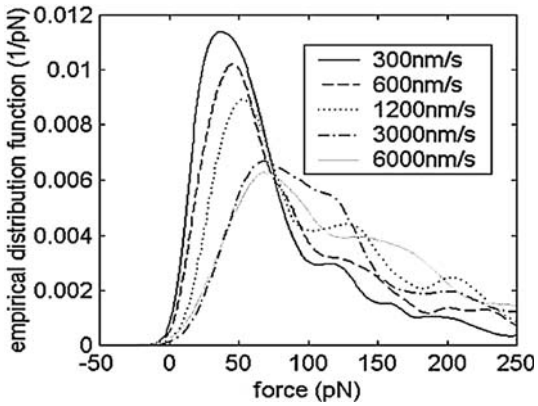

Fig. 4 Distribution of unbinding forces of Dsg1-Fc *trans*-interactions. The individual curves correspond to different pulling velocities (force loading rates). The interaction time of tip and sample was kept constant at 1 s. The observed unbinding forces are distributed in clusters (distinct peaks in the distribution) approximately around multiples of a unitary force. With higher force loading rates, the individual force peaks (center of the force clusters) are shifted to higher values and the occupation of the force clusters is significantly changed; i.e., higher forces are more frequent

plot shown in Figure 3 represents the mean activity of at least 500 subsequent retrace cycles. Four different tips were used, all yielding the same degree of Ca^{2+} dependence. Binding activity (*trans*-interaction between tip- and substrate-bound Dsg1) showed half-maximal adhesion activity at 0.8 mM Ca^{2+} (apparent K_d) with a high degree of cooperativity (Hill coefficient $n_h > 5$). These experiments show that Dsg1 exhibits Ca^{2+}-dependent homophilic binding which is negligible below 0.7 mM Ca^{2+} and maximal at 1 mM Ca^{2+}.

Lifetime of *Trans*-Interacting Dsg1

The general principle for determining unbinding forces and lifetimes of bonds of *trans*- interacting recombinant cadherin dimers has been described in detail previously (Baumgartner et al., 2000). Cadherins covalently attached to the tip of the cantilever and to the surface of the substrate are repeatedly brought into contact and separated by cyclic up- and downward movements of the tip at velocities of 300–6000 nm/s over a distance of 300 nm (force-distance cycles). For correct kinetic evaluation, the time interval in which the Dsg1 proteins can interact (tip-substrate interaction time) was kept constant at 1 s. Only the final unbinding event during which the cantilever jumped to the neutral, undeflected position was taken for statistical analysis. The distribution curves of unbinding forces under these conditions are depicted in Figure 4. It is apparent that the unbinding forces are distributed in clusters (distinct peaks in the distribution) around multiples of a unit force. When increasing the pulling velocity, not only the individual force peaks (center of the force clusters) are shifted to higher values but also the occupation of the force clusters is significantly changed. This is clearly visible from a detailed analysis of the first cluster (minimal force), using a recently developed deconvolution algorithm (Baumgartner & Drenckhahn, 2002). Figure 5A shows the dependence of the minimal unbinding force on the pulling velocity. When increasing the pulling velocity from 300 to 6,000 nm/s, unbinding forces increased from 37 to 68 pN. According to Bell's equation (Bell, 1978), this allows determination of the lifetime of the single bond to be approximately 0.17 s ($k_{off} = 5.88\ s^{-1}$). This lifetime is significantly smaller than the lifetimes determined by the same approach for N-cadherin (Baumgartner et al., 2003), VE-cadherin (Baumgartner et al., 2000), E-cadherin and LI-cadherin (Baumgartner et al., *unpublished data*), which for all these cadherins is about 1 s (0.7–1.3). However, in contrast to the other cadherins tested so far, there is a remarkable shift of the occupation of the different force clusters. The percentage of interaction forces which belong to the minimal force cluster is depicted in Figure 5B in dependence on the pulling velocity. As clearly visible from this graph, there is a monoexponential decrease of the occupation of the minimal force cluster in dependence on the pulling velocity. The simplest way to explain this behavior is to assume a multivalent interaction of individual Dsg1 cadherins with two or more sites at the ectodomain. This means that if the pulling velocity is slow, successive unbinding of complex bonds takes place, whereas in the case of high pulling velocities the complex bonds have no time to break successively. If independent multivalent binding is assumed, the actual number of bonds between two *trans*-interacting Dsg1 molecules should be distributed binomially after 1 s of tip-sample interaction. If we further assume that new bonds will not form during stretching of the molecule, we can find the probability for the occupation of the minimal force cluster (one single bond) to be

$$p(N_r = 1)\sum_{i=1}^{N} p(N_r = 1|N_0 = i).p(N_0 = i)$$

where N_r is the number of bonds at the rupture, N is the maximum number of bonds and N_0 is the number of bonds at the end of direct tip-sample interaction. If no rebinding occurs, the probability of N_r follows to be

$$p(N_r = 1|N_0 = i) = i \cdot e^{-t/\tau} \cdot (1 - e^{-t/\tau})^{(i-1)}$$

with t representing the time between tip-sample separation and rupture and τ standing for the lifetime of a single bond.

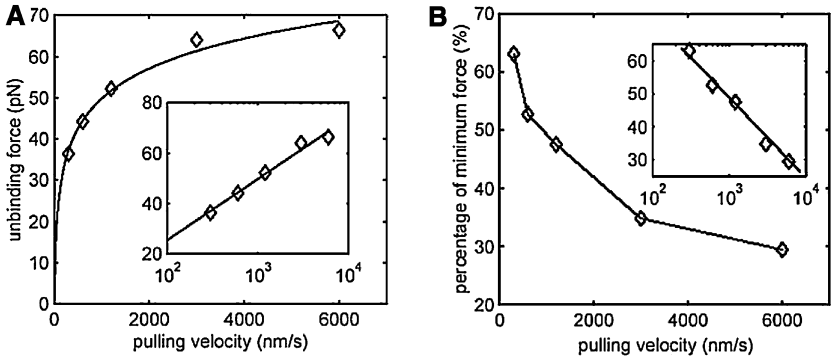

Fig. 5 Analysis of the first cluster (minimal force) of the Dsg1-Fc *trans*-interaction. A clear exponential dependence of the minimal unbinding force on the pulling velocity is observed (**A**). Forces range 37–68 pN when increasing the pulling velocity from 300 to 6,000 nm/s, yielding a lifetime of a single bond of approximately 0.17 s. Analysis of the occupation frequency of the individual force clusters shows a remarkable shift of the percentage of interaction forces which belong to the minimal force cluster (**B**) in dependence on the pulling velocity. A monoexponential decrease of the occupation of the minimal force cluster in dependence on the pulling velocity can be observed

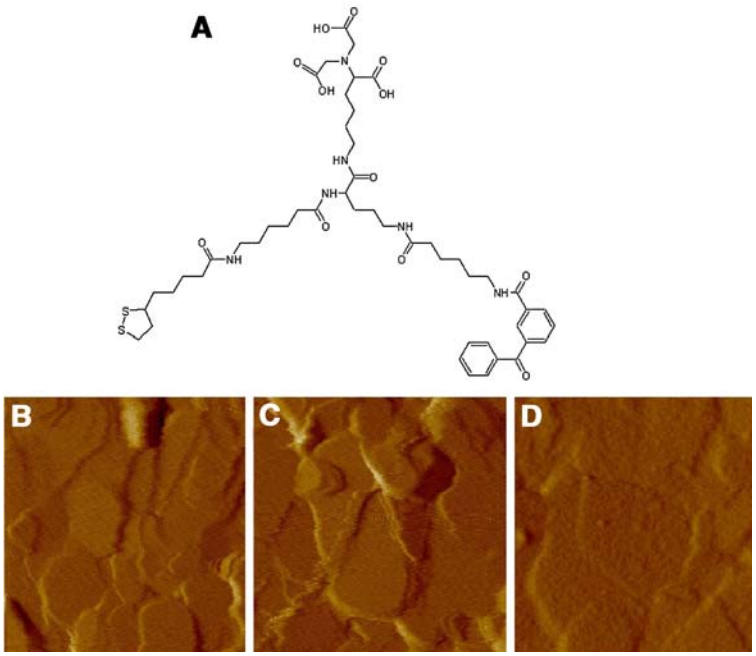

Fig. 6 SAMs containing the trifunctional linker LLAB. (**A**) Schematic of the linker containing an NTA, a lipoic acid and a benzophenone group. A mixture of this linker with lipoic acid amide was used to form SAMs on gold surfaces. AFM deflection images of the flame annealed gold (**B**), of the SAM (**C**) and of the SAM after binding of Dsg1-Fc-His6 (**D**) prove the working principle of the surface modification procedure

The probability of the number of bonds at the time of tip-sample separation is given as

$$p(N_0 = i) = \binom{N}{i} . p_b^i . (1 - p_b)^{(N-i)} . (1 - p_b)^{-N}$$

where p_b equals the probability of one bond forming at the time of tip-sample separation. The last term accounts for the censuring of the data; i.e., if no bond is available at the time of tip-sample separation, no event will be observed within the force-distance cycle and the cycle will be excluded from analysis. Using this description, the decrease of the occupation of the minimal force cluster corresponds to a lifetime of the individual bond of approximately 0.12 s, which is in good agreement with the lifetime of the individual bond found from the analysis of the minimal force cluster (0.17 s) as outlined above. Thus, this result suggests that homophilic binding of two Dsg1 molecules displays several independent interactions of approximately equal binding strength.

Overlapping of *Trans*-Interacting Dsg1 Molecules

To directly show multivalent interactions and to specify the degree of overlap of the *trans*-interacting Dsg1 molecules, the AFM setup has to be modified to couple Dsg1-Fc in a

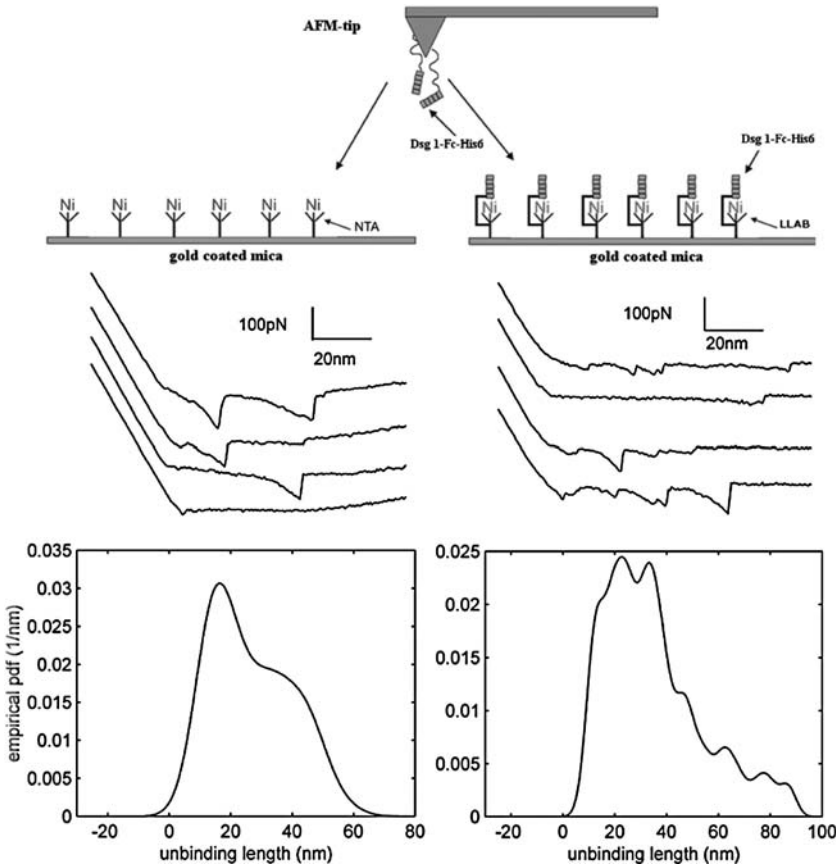

Fig. 7 Selection of an AFM tip containing only two Dsg1-Fc-His6 molecules and application of this tip on SAM-linked Dsg1. Application of a tip on a surface containing NTA-bound Ni ions yields typical force-distance curves showing unbinding events at two distinct positions and all at about the same unbinding force of approximately 90 pN. If the same tip is applied on a SAM with directly attached Dsg1-Fc-His6 molecules, all tethered covalently at their C-terminal end via LLAB, a broad distribution of unbinding length is obtained. This can be explained either by assuming different degrees of overlap of the individual molecules or by conformational changes

predictable orientation to the substrate. Instead of coupling Dsg1-Fc randomly via flexible PEG chains, we developed a method to couple Dsg1-Fc covalently to lipid elements of SAMs via its C-terminal end. For this purpose, mixtures of lipoic acid amide and lysine-N_{ε}-lipoic acid-N_{α}-aminohexylbenzophenone (LLAB) were allowed to form SAMs on gold-coated mica sheets as described in Materials and Methods. NTA amine was then coupled to the carboxyl group of the lysine-*N*-lipoic acid-*N*-aminohexylbenzophenone to generate a trifunctional linker (schematic in Fig. 6A). The NTA/Ni group serves as binding site for the His6 portion at the C terminus of the Fc portion of the Dsg1-Fc-His_6 protein, forcing the bound fusion protein in well-defined orientation with the ectodomain pointing away from the substrate. Covalent linkage between the gold-attached LLAB linker and the Dsg1-Fc-His6 fusion protein was induced by UV activation of the photoreactive benzophenone group. Due to the short length of the benzophenone-containing side chain covalent coupling will be most likely located in close vicinity to the C terminus of the Fc portion. As shown by AFM images in Figure 6, the SAM (Fig. 6C) did not change the topography of the gold surface compared to the pure uncoated gold surface (Fig. 6B). After coupling of the protein to the SAM, a change of topography is clearly visible (Fig. 6D) as distinct bumps appear which correspond to individual Dsg1 molecules. If UV illumination was omitted, the protein coverage could be completely washed off the surface using imidazole or EGTA (*data not shown*).

In order to obtain information on the number of Dsg1 groups attached to the cantilever tip, individual cantilevers functionalized with PEG-linked Dsg1-Fc-His6 were tested by force-distance cycles on a SAM with LLAB containing NTA^{-}/Ni^{+} head groups. This screening method allowed selection of cantilevers with one or two Dsg molecules attached to the accessible tip area. Figure 7 shows an experiment of 800 force-distance cycles with maximally two unbinding events with two different well-defined unbinding lengths occurring in individual cycles. The force distribution shows only one clear peak at about 90 pN, which is slightly below recently published values for the unbinding forces of NTA-Ni-His6 bonds (*not shown*). Thus, the experiments shown in Figure 7 can be taken as proof that only two well-separated Dsg1 molecules are attached to the AFM tip in the accessible tip area. The same cantilever was then applied on a SAM containing Dsg1-Fc-His6 covalently linked to the gold surface by the LLAB linker. On this surface, multiple (up to five) distinct unbinding events occurred with a broad distribution of unbinding lengths (Fig. 7, right) as well as clustered force

distribution similar to that observed with PEG-linked Dsg1 (*see above*). Although the geometry of the substrate-bound, Dsg1-Fc-His6-bound molecules is well defined and homogeneous, the linkage of the PEG-bound fusion proteins attached to the tip remained variable. Thus, absolute values of overlap between interacting tip- and substrate-bound Dsg1 molecules could not be determined. However, these experiments clearly show that multivalent types of interaction occurred with a variety of unbinding lengths.

Discussion

In this study, we characterized for the first time the molecular binding properties of Dsg1 and provide evidence that the mechanisms of Dsg1-mediated *trans*-interaction partly differ from other members of the cadherin superfamily studied by the same technical approach. It has been proposed that desmogleins predominantly bind in a heterophilic way to desmocollins (Dsc), the second family of desmosomal cadherins. Based on cell aggregation assays, immunoprecipitation or studies with soluble fragments of the external domain of Dsg1, it has been assumed that homophilic binding of desmogleins must be weak or even negligible (Amagai et al., 1994; Chitaev & Troyanovsky, 1997; Runswick et al., 2001; Syed et al., 2002). In contrast to these studies, we here unequivocally demonstrate that Dsg1 undergoes specific homophilic *trans*-interactions. Homophilic interaction has been already shown for Dsg3 (Amagai et al., 1994). However, it has to be emphasized that the *in vitro* conditions of our assay may not completely apply to the situation *in vivo*, and thus, a final conclusion about the relevance of homophilic Dsg1-mediated adhesion *in vivo* is not possible.

Heterophilic Dsg1 binding to other desmocadherins like Dsc1 or Dsc2a has been reported in previous studies using aggregation assays of transfected cells (Runswick et al., 2001). Nevertheless, from these studies no kinetic information about the heterophilic binding mechanism could be determined.

AFM experiments using fusion proteins containing the complete extracellular domain of human Dsg1 reveal *trans*-interaction of tip- and plate-bound Dsg1 molecules which was reduced to background levels in the absence of Ca^{2+}. This behaviour was not observed when Ba^{2+} was used instead of Ca^{2+}. In a previous study, we have shown that a monoclonal Dsg1 antibody inhibits Dsg1 *trans*-interaction, showing that Dsg1 binding is a specific event (Waschke et al., 2005).

In the present study, we found that the binding activity depends on Ca^{2+} in a highly cooperative manner ($n_h > 5$) at a K_d (half-maximal activity) of about 0.8 mM Ca^{2+}. The Ca^{2+} dependence of VE-cadherin and N-cadherin was determined recently (Baumgartner et al., 2000, 2003). It is remarkable that the specific combinations of K_d (0.72 mM Ca^{2+} for N-cadherin and 1.1 mM Ca^{2+} for VE-cadherin) and the Hill coefficient (~2 for N-cadherin and ~5 for VE-cadherin) differ significantly from the combination determined for Dsg1. These data suggest that VE-cadherin displays nearly an "all-or-nothing" transition close to the physiological Ca^{2+} level, whereas N-cadherin is less sensitive to the extracellular Ca^{2+} concentration ($[Ca^{2+}]_e$) and displayed a moderate degree of cooperativity, which would allow a graded response of adhesive activity over a broader range of $[Ca^{2+}]_e$. Dsg1, on the other hand, behaves like VE-cadherin in the sense of "all-or-nothing" but not that close to the physiological $[Ca^{2+}]_e$ level. This Ca^{2+} dependence of Dsg1 *trans*-interaction may be of major biological importance. It has been reported that the human epidermis displays a calcium gradient with low calcium in the lower basal and spinous layers and highest levels in the stratum granulosum (Elias et al., 2002; Menon & Elias, 1991). Thus, our data indicate that not only the expression levels of Dsg1 in the specific layers but also the calcium level might regulate Dsg1-mediated adhesion if homophilic adhesion of Dsg1 significantly contributes to desmosomal adhesion *in vivo*. The contribution of homophilic Dsg1 binding to desmosomal adhesion would be less in the lower epidermis compared to more superficial layers. This is of medical relevance because different forms of pemphigus disease affect certain levels of the epidermis (Amagai, 2003; Bystryn & Rudolph, 2005). Moreover, pemphigus skin blistering results in a local breakdown of epidermal barrier functions, leading to loss of the epidermal Ca^{2+} gradient similar to an artificially induced epidermal lesion (Elias et al., 2002). The altered Ca^{2+} concentration would in turn lead to a loss of Dsg1-mediated binding, especially in the superficial epidermis. This mechanism could aggravate skin blistering in addition to the autoantibody-mediated effects on Dsg1 binding (Waschke et al., 2005).

Force measurements revealed clustering of unbinding forces as multiples of a unitary force, similar to recent observations using other members of the cadherin superfamily. The forces observed were strictly dependent on the pulling velocity (force loading rate). Most interestingly, the occupancy of the different force clusters was also velocity-dependent such that higher force clusters were populated at higher pulling velocities. This strengthens the view of multivalent interactions as proposed by different groups in recent years (Ahrens et al., 2003; Leckband, 2002; Leckband & Prakasam, 2006; Legrand et al., 2001; Pertz et al., 1999; Pokutta et al., 1994; Sivasankar et al., 1999; Sivasankar, Gumbiner & Leckband, 2001; Tomschy et al., 1996). Detailed analysis of the unbinding behavior is in good agreement with a model assuming several independent interactions between individual *trans*-interacting

Dsg1-Dsg1 pairs. However, this is in contrast to analysis done with other types of cadherins, like VE- or N-cadherin. Under the same conditions, these proteins exhibited homophilic interactions showing a significantly longer lifetime and no measurable shift of the occupancy of the force clusters (*not shown*). The multivalent interactions correspond to different geometries as evident from the analysis of unbinding length. This may be due to different degrees of overlap or to conformational changes.

Despite the rather similar secondary and tertiary structures, substantial differences with respect to their molecular binding properties between the various cadherin members have been observed, as outlined above. In recent years, several studies have been published on the structure and function of cadherins. Several of these publications led to a rather polemic discussion on the validity of methods used for the investigation as well as models of cadherin-cadherin interaction. Using the identical approach of single-molecule force spectroscopy for different cadherins, we found remarkable differences between the cadherins investigated so far, i.e., VE-cadherin, N-cadherin, LI-cadherin and now Dsg1. These findings support recent data from Wirtz and colleagues, who also found that E-cadherin, N-cadherin and VE-cadherin exhibit different biomechanical properties (Panorchan, George & Wirtz, 2006a; Panorchan et al., 2006b). Thus, the general mode of *trans*-interaction of members of the classical cadherin superfamily appears to underly significant type-specific variations, rendering individual approaches for all types of cadherins necessary.

Acknowledgements We are grateful to Gabriele Königer and Agnes Weth for excellent technical assistance. The study was supported by grants from the Deutsche Forschungsgemeinschaft (SFB 487, TP B5) and the Austrian Science Foundation (P15295).

References

Ahrens T, Lambert M, Pertz O, Sasaki T, Schulthess T, Mege RM, Timpl R, Engel J (2003) Homoassociation of VE-cadherin follows a mechanism common to "classical" cadherins. J Mol Biol 325:733–742

Amagai M (2003) Desmoglein as a target in autoimmunity and infection. J Am Acad Dermatol 48:244–252

Amagai M, Karpati S, Klaus-Kovtun V, Udey MC, Stanley JR (1994) Extracellular domain of pemphigus vulgaris antigen (desmoglein 3) mediates weak homophilic adhesion. J Invest Dermatol 103:609–615

Amagai M, Matsuyoshi N, Wang ZH, Andl C, Stanley JR (2000) Toxin in bullous impetigo and staphylococcal scalded-skin syndrome targets desmoglein 1. Nat Med 6:1275–1277

Baumgartner W, Drenckhahn D (2002) An expectation-maximisation algorithm for the deconvolution of the intrinsic distribution of single molecule's parameters. Comput Chem 26:321–326

Baumgartner W, Golenhofen N, Grundhofer N, Wiegand J, Drenckhahn D (2003) Ca^{2+} dependency of N-cadherin function probed by laser tweezer and atomic force microscopy. J Neurosci 23:11008–11014

Baumgartner W, Hinterdorfer P, Ness W, Raab A, Vestweber D, Schindler H, Drenckhahn D (2000) Cadherin interaction probed by atomic force microscopy. Proc Natl Acad Sci USA 97:4005–4010

Bell GI (1978) Models for the specific adhesion of cells to cells. Science 200:618–627

Bystryn JC, Rudolph JL (2005) Pemphigus. Lancet 366:61–73

Chan WC, White PD (2003) Fmoc Solid Phase Peptide Synthesis. New York: Oxford UNiversity Press

Chitaev NA, Troyanovsky SM (1997) Direct Ca^{2+}-dependent heterophilic interaction between desmosomal cadherins, desmoglein and desmocollin, contributes to cell-cell adhesion. J Cell Biol 138:193–201

Elias P, Ahn S, Brown B, Crumrine D, Feingold KR (2002) Origin of the epidermal calcium gradient: regulation by barrier status and role of active vs passive mechanisms. J Invest Dermatol 119:1269–1274

Garrod DR, Merritt AJ, Nie Z (2002) Desmosomal cadherins. Curr Opin Cell Biol 14:537–545

He W, Cowin P, Stokes DL (2003) Untangling desmosomal knots with electron tomography. Science 302:109–113

Hinterdorfer P, Baumgartner W, Gruber HJ, Schilcher K, Schindler H (1996) Detection and localization of individual antibody-antigen recognition events by atomic force microscopy. Proc Natl Acad Sci USA 93:3477–3481

Kottke MD, Delva E, Kowalczyk AP (2006) The desmosome: cell science lessons from human diseases. J Cell Sci 119:797–806

Leckband D (2002) The structure of the C-cadherin ectodomain resolved. Structure 10:739–740

Leckband D, Prakasam A (2006) Mechanism and dynamics of cadherin adhesion. Annu Rev Biomed Eng 8:259–287

Legrand P, Bibert S, Jaquinod M, Ebel C, Hewat E, Vincent F, Vanbelle C, Concord E, Vernet T, Gulino D (2001) Self-assembly of the vascular endothelial cadherin ectodomain in a Ca^{2+}-dependent hexameric structure. J Biol Chem 276:3581–3588

Mahoney MG, Wang Z, Rothenberger K, Koch PJ, Amagai M, Stanley JR (1999) Explanations for the clinical and microscopic localization of lesions in pemphigus foliaceus and vulgaris. J Clin Invest 103:461–468

Menon GK, Elias PM (1991) Ultrastructural localization of calcium in psoriatic and normal human epidermis. Arch Dermatol 127:57–63

Merrifield RB (1964) Solid-phase 127peptide synthesis. 3. An improved synthesis of bradykinin. Biochemistry 3:1385–1390

Miyagawa S, Amagai M, Iida T, Yamamoto Y, Nishikawa T, Shirai T (1999) Late development of antidesmoglein 1 antibodies in pemphigus vulgaris: correlation with disease progression. Br J Dermatol 141:1084–1087

Panorchan P, George JP, Wirtz D (2006a) Probing intercellular interactions between vascular endothelial cadherin pairs at single-molecule resolution and in living cells. J Mol Biol 358:665–674

Panorchan P, Thompson MS, Davis KJ, Tseng Y, Konstantopoulos K, Wirtz D (2006b) Single-molecule analysis of cadherin-mediated cell-cell adhesion. J Cell Sci 119:66–74

Payne AS, Hanakawa Y, Amagai M, Stanley JR (2004) Desmosomes and disease: pemphigus and bullous impetigo. Curr Opin Cell Biol 16:536–543

Pertz O, Bozic D, Koch AW, Fauser C, Brancaccio A, Engel J (1999) A new crystal structure, Ca^{2+} dependence and mutational analysis reveal molecular details of E-cadherin homoassociation. EMBO J 18:1738–1747

Pokutta S, Herrenknecht K, Kemler R, Engel J (1994) Conformational changes of the recombinant extracellular domain of E-cadherin upon calcium binding. Eur J Biochem 223:1019–1026

Runswick SK, O'Hare MJ, Jones L, Streuli CH, Garrod DR (2001) Desmosomal adhesion regulates epithelial morphogenesis and cell positioning. Nat Cell Biol 3:823–830

Sieber P (1987) Anchoring of Fmoc-amino acids with T3P. Tetrahedron Lett 28:6147–6150

Sitaru C, Zillikens D (2005) Mechanisms of blister induction by autoantibodies. Exp Dermatol 14:861–875

Sivasankar S, Brieher W, Lavrik N, Gumbiner B, Leckband D (1999) Direct molecular force measurements of multiple adhesive interactions between cadherin ectodomains. Proc Natl Acad Sci USA 96:11820–11824

Sivasankar S, Gumbiner B, Leckband D (2001) Direct measurements of multiple adhesive alignments and unbinding trajectories between cadherin extracellular domains. Biophys J 80:1758–1768

Stanley JR, Amagai M (2006) Pemphigus, bullous impetigo, and the staphylococcal scalded-skin syndrome. N Engl J Med 355:1800–1810

Syed SE, Trinnaman B, Martin S, Major S, Hutchinson J, Magee AI (2002) Molecular interactions between desmosomal cadherins. Biochem J 362:317–327

Tomschy A, Fauser C, Landwehr R, Engel J (1996) Homophilic adhesion of E-cadherin occurs by a co-operative two-step interaction of N-terminal domains. EMBO J 15:3507–3514

Wang SS, Merrifield RB (1969) Preparation of some new biphenylisopropyloxycarbonyl amino acids and their application to the solid phase synthesis of a tryptophan-containing heptapeptide of bovine parathyroid hormone. Int J Protein Res 1:235–244

Waschke J, Bruggeman P, Baumgartner W, Zillikens D, Drenckhahn D (2005) Pemphigus foliaceus IgG causes dissociation of desmoglein 1-containing junctions without blocking desmoglein 1 transinteraction. J Clin Invest 115:3157–3165

Waschke J, Spindler V, Bruggeman P, Zillikens D, Schmidt G, Drenckhahn D (2006) Inhibition of Rho A activity causes pemphigus skin blistering. J Cell Biol 175:721–727